

SALA: Soft Assignment Local Aggregation for 3D Semantic Segmentation

Hani Itani Silvio Giancola Ali Thabet Bernard Ghanem

King Abdullah University of Science and Technology (KAUST)

{hani.itani.2, silvio.giancola, ali.thabet, bernard.ghanem}@kaust.edu.sa

Abstract

We introduce the idea of using learnable neighbor-to-grid soft assignment in grid-based aggregation functions for the task of 3D semantic segmentation. Previous methods in literature operate on a predefined geometric grid such as local volume partitions or irregular kernel points. These methods use geometric functions to assign local neighbors to their corresponding grid. Such geometric heuristics are potentially sub-optimal for the end task of semantic segmentation. Furthermore, they are applied uniformly throughout the depth of the network. A more general alternative would allow the network to learn its own neighbor-to-grid assignment function that best suits the end task. Since it is learnable, this mapping has the flexibility to be different per layer. This paper leverages learned neighbor-to-grid soft assignment to define an aggregation function that balances efficiency and performance. We demonstrate the efficacy of our method by reaching state-of-the-art (SOTA) performance on S3DIS with almost $10\times$ less parameters than the current reigning method. We also demonstrate competitive performance on ScanNet and PartNet as compared with much larger SOTA models.

1. Introduction

Point cloud semantic segmentation is one of the fundamental tasks of 3D scene understanding. This task provides an holistic view of a scene by grouping points according to their class labels. In an analogous way, 2D semantic segmentation performs grouping of pixels into semantically meaningful classes. In image space, Convolutional Neural Networks (CNNs) are the de-facto solution to most 2D image understanding tasks including 2D semantic segmentation. Extending CNNs to point cloud tasks is challenging, given the intrinsic differences with images. Point sets are unordered and permutation invariant. This is a consequence of how points are localized, mainly by their XYZ coordinates instead of indices in a regular 2D grid seen in images. Furthermore, point clouds are characterized by an uneven point density distribution over the volume they oc-

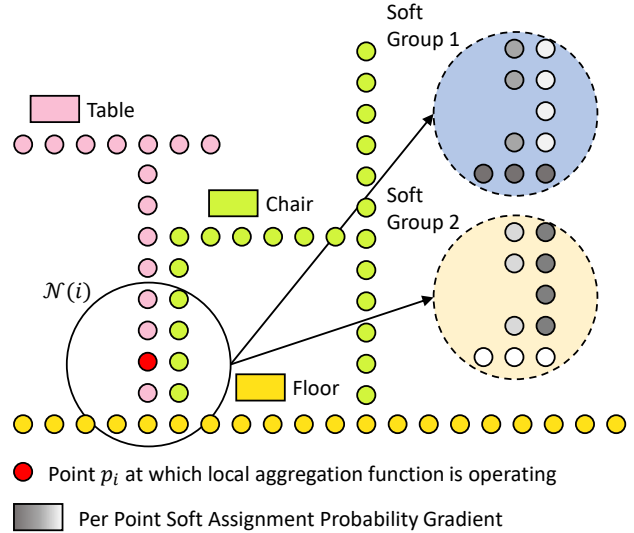


Figure 1. **Neighbor Point Soft Assignment.** We propose to use learnable soft assignment when aggregating over a neighborhood $\mathcal{N}(i)$ using a grid-based local aggregation function to update the feature of a point p_i . This is especially useful when a geometric assignment is not intuitive. The schematic shows 2 groups only, but the assignment is valid for any S number of groups.

cupy. For these reasons, discrete kernel convolutions, which are the building blocks of 2D CNNs, cannot be applied directly on point clouds. Efforts exist to project point clouds into multiple 2D images, which can be fed into standard CNNs [22]. Alternatively, one can voxelize a point cloud to obtain a regular 3D grid that can be processed by a 3D CNN [16].

A more intuitive approach is to devise networks that operate directly on points. These so called point-processing networks are categorized as either global or local neighborhood aggregation methods. As the name suggests, global methods aggregate information from the entire point cloud and fail to capture local contextual details. On the other hand, local neighborhood methods address this problem by defining a point neighborhood, over which information is aggregated (Figure 1). A typical approach in the local category encompasses grid-based methods, which share a similar flavor to image convolutions. These methods introduce a

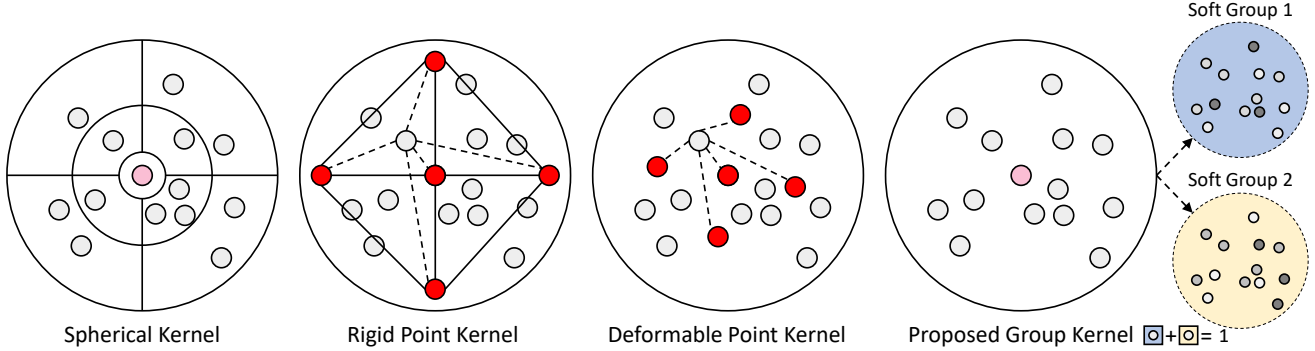


Figure 2. **Comparison of Spatial Grid Kernels as Opposed to our Non-spatial Defined Kernel.** There exists several spatial grid kernels in literature. Spherical Kernels [10, 9] are defined by regular spherical partitions. On the other hand, both rigid and deformable Point Kernels [24] are irregular, since they rely on spatially defined kernel points (red). Unlike rigid point kernels, a deformable kernel adapts its kernel points configuration based on locality. These grid kernels are accompanied by a geometric neighbor-to-grid mapping function. In our case, having a learnable assignment function eliminates the need for a spatially defined kernel. Instead, we define groups, each with its own kernel weight. The rightmost figure shows an example of a group kernel with two groups, whereby each neighbor point is endowed with two group membership scores (add up to one) used in aggregation. Clearly, any number of groups can be used.

grid kernel, with cells defined by their spatial grid location and a kernel weight. To operate on point neighborhoods, grid-based methods need to first define the spatial geometry of the grid kernel, as well as the neighbor-to-grid assignment, *i.e.*, which kernel weights interact with each neighbor point. Both these operations are currently pre-defined using a set of geometric heuristics. For example, [10] proposes to use spherical neighborhood partitions as grid cells and assigns kernel weights to neighbor points based on the partition they occupy (see Figure 2).

In this work, instead of relying on geometric heuristics, we propose to *learn* the neighbor-to-grid assignment. By learning such an assignment, we do not need to spatially define our grid kernel. Instead, we compose a group-based kernel that consists of groups, to which neighbors are assigned. This kernel enjoys the flexibility of being irregular, unstructured, and non-spatial (see Figure 2). Furthermore, neighbor points are assigned to groups in a soft manner, *i.e.* each point belongs to all groups with a learned membership metric. By giving the local aggregation function this flexibility, it can learn an adaptive and a more general neighbor point assignment, superior to its geometric counterpart. Our function learns to group neighbor features in a way that best suits the end task of semantic segmentation with no local spatial constraints. We demonstrate the effectiveness of our group-based kernel by formulating a **Soft Assignment based Local Aggregation (SALA)** function (Figure 2). SALA is integrated into the unified framework proposed by [15] for the task of 3D semantic segmentation of indoor scenes and shapes. With this setup, we show how SALA achieves SOTA performance on S3DIS using almost $10\times$ less parameters than previous methods. We also present very competitive results on ScanNet and PartNet benchmarks, when compared with much bigger models.

Contributions: (i) We define a novel aggregation called the **Soft Assignment Local Aggregation (SALA)** function, which is endowed with a learnable and non-spatial grid kernel. SALA offers the flexibility of softly assigning neighborhood points to a grid, it can learn optimal point memberships and enhance the downstream task of point cloud semantic segmentation. (ii) We demonstrate the efficacy of SALA on 3D scene and shape part segmentation tasks. We achieve SOTA in S3DIS and competitive results in ScanNet and PartNet, while using $10\times$ and $3\times$ fewer parameters for scene and shape part segmentation, respectively.

2. Related Work

Image- and Voxel-Based Methods. These methods derive an intermediate representation of point clouds that can be processed by CNNs for 3D point cloud understanding tasks. Image-based methods project a point cloud onto 2D images either using multiple global [22, 8, 19] or many local tangential view points [23]. Projecting a point cloud into 2D may result in a very sparse image depending on local point density. Furthermore, local geometric information important for semantic segmentation is compromised, if the view points are not carefully selected [6]. In comparison, voxel-based methods leverage the regularity of 3D voxels, on which 3D CNNs can operate [19, 16]. These methods are generally memory expensive despite being limited to relatively small 3D CNN kernel sizes. Furthermore, a voxel representation uses a fixed size grid throughout a scene, including empty spaces. Alternatively, other methods operate on Octrees [27, 21] that use an adaptive voxel grid size determined by local point density. Other methods leverage the sparsity of voxel representations by operating on hash tables [3, 31] for very efficient feature learning.

Point-Based Methods. Point processing methods operate directly on point clouds, they can be classified into global and local methods. PointNet [18] is among the first works for deep learning on un-ordered point clouds. It is a global pointwise method, it processes neighbor features independently and aggregates information globally by reducing over the entire point cloud through a symmetric aggregation operator. Local methods operate on local neighborhoods instead and can be categorized into three categories:

Pointwise-MLP Methods. PointNet++ [20] extends PointNet to capture local geometries and contextual relationships by reducing over local spatial neighborhoods instead. Local pointwise-MLP methods such as [20, 28, 12] treat all neighbors equally and are agnostic of the diversity or redundancy of information in a given neighborhood.

Attention-Based Methods. These methods process neighbor points similar to local pointwise-MLP methods, but replace the simple reduction function by learnable weighted sum. These weights are generated from a series of transformations on geometric features, such as position [14] and local point density [29]. Alternatively, they use neighbor feature to derive attention aggregation weights [26, 5], similar to graph attention networks [25]. The reduction function is still symmetric, unaffected by permutation. By applying an attention on the neighbor features, the local aggregation function would learn to highlight the important neighbors depending on their relevance to learning the end task learning. Our learnable soft assignment is a form of attention that tells a group which neighbors to consider for aggregation.

Grid-Based Methods. These methods attend to neighborhood diversity by projecting a local neighborhood onto a grid kernel. The differentiating factor among these methods is the defined spatial grid and its accompanying neighbor-to-grid mapping function. [10] uses a spherical kernel defined by partitioning a local spherical neighborhood along the spherical coordinates. Neighbor points are then processed by the single kernel weight of the partition they occupy. [9] addresses the problem of weight discontinuity at boundary points between partitions by combining the kernel weights of surrounding partitions. [24] introduces kernel point convolutions on local neighborhoods. Kernel points can be regarded as an irregular spatial grid defined by points in a particular configuration. It processes every neighbor point with a weight derived as a linear combination of all kernel weights. The contribution of a kernel weight to a neighbor point is defined by its spatial proximity to the pre-defined kernel point. [24] also offers a deformable point kernel that learns to shift its initial kernel point configuration per locality. A learned neighbor-to-grid assignment allows the local aggregation function to explore neighbor interactions beyond spatial similarity heuristics. More importantly, it enables the formation of non-spatial and unstructured kernels, which adapt to each locality.

3. Methodology

3.1. Definitions

A point cloud is defined by its 3D coordinates $\mathcal{P} \in \mathbb{R}^{N \times 3}$ and a corresponding set of features $\mathcal{F} \in \mathbb{R}^{N \times C_{in}}$. Given a point $p_i \in \mathcal{P}$, a local aggregation function updates its feature $f_i \in \mathcal{F}$ by aggregating information over a local neighborhood $\mathcal{N}(i)$. A grid-based local aggregation function is defined by a kernel of size S and a set of kernel weights $\{W_g\}_{g=0}^{S-1}$ used to encode neighbor features. Previous methods used spatial kernels such as regular spherical partitions or irregular point kernels. An assignment function $h(\cdot)$ maps a neighbor point $j \in \mathcal{N}(i)$ to its corresponding kernel weight. Due to the spatial nature of the kernel, the neighbor-to-grid assignment function $h(\cdot)$ is of a geometric nature, based on spatial similarity heuristics. The output of $h(\cdot)$ can either be hard assignment by selecting a single kernel weight [10], or soft assignment by combining several of them [9, 24]. The resulting neighbor encoding weight per grid unit is referred to as $W_{j,g}$ (1). The updated feature $f'_{i,g}$ of a center point per grid unit is then obtained by reducing over the set of encoded neighbor features using a symmetric operator $R(\cdot)$. The symmetry of $R(\cdot)$ accounts for the permutation invariance property of point clouds (2). The final updated center node feature f'_i is obtained by channel-wise sum across the updated center features per grid unit (3). For a grid convolution, $R(\cdot)$ is set to SUM.

$$W_{j,g} = h(p_j, g)W_g \quad (1)$$

$$f'_{i,g} = R(\{W_{j,g}f_j \mid j \in \mathcal{N}(i)\}) \quad (2)$$

$$f'_i = \sum_{g < S} f'_{i,g} \quad (3)$$

We propose to use a learnable soft assignment of neighbors to replace the geometric neighbor-to-grid assignment function $h(\cdot)$ used in previous local grid-based methods. Our learnable soft assignment function gives us an advantage over previous grid kernels because it allows for a non-spatial kernel definition. As a consequence, we propose to use a group kernel defined by a pre-set number of non-spatial and unstructured groups. A group is analogous to a point in a point kernel or a partition in a spherical kernel. The proposed learnable soft assignment function regresses the membership probabilities of neighbor points to each group. The assignment function would learn to group neighbor points whose semantic interaction leads to an improved feature update for the considered point.

3.2. SALA Formulation

Operations in SALA are outlined in Figure 3. Similar to grid-based methods, every group has its own learnable

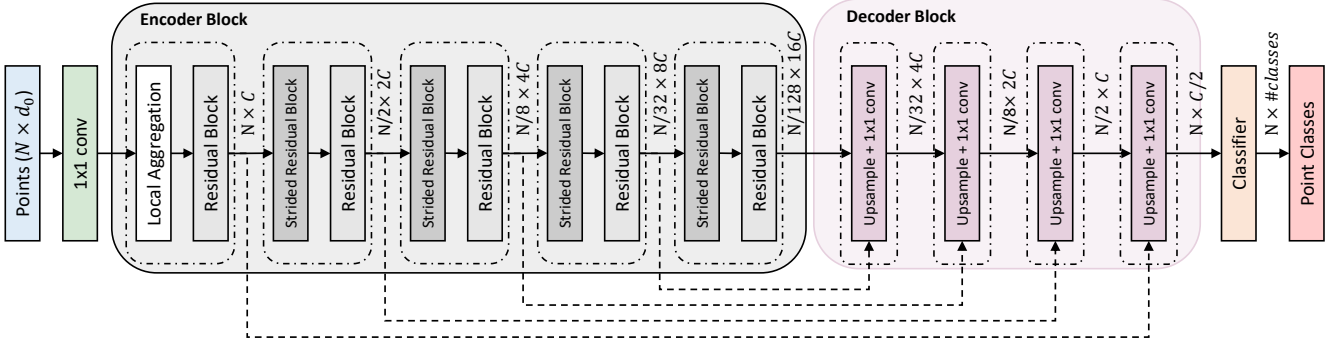


Figure 4. **Architecture.** Unified architecture framework from [15]. Both Residual and Strided Residual Blocks have local aggregation functions within. The strided residual blocks acts as a pooling operator in which point cloud resolution is reduced using grid-subsampling. The grid size is doubled going deeper in the encoder. C refers to channel output of first encoding layer.

$$h(r_j, \tilde{x}_g) = \text{MAX} \left(0, 1 - \frac{\|r_j - \tilde{x}_g\|_2}{\sigma} \right) \quad (12)$$

$$f'_i = \sum_{j < k} \sum_{g < S} h(p_j, \tilde{x}_g + \Delta_{p_i}) W_g f_j \quad (13)$$

By comparing equations (10) and (13), one observes that the group kernel in SALA shares some similarities with the deformable point kernel in [24]. Instead of learning shifts of kernel points, we learn to assign neighbors to non-spatial groups using a learnable assignment function $h(\cdot)$ (5). Similar to a deformable kernel, our learnable function adapts per locality. An additional advantage of SALA over previous methods is that it can learn a different mapping function per layer. The learned assignment will therefore be driven by the performance on the end task.

3.4. Architecture

Recently, [15] shows that the different types of local aggregation functions can reach comparable SOTA performance on several datasets. It uses a similar architecture as proposed in [24], as well as similar data preprocessing, training, and testing schemes. For a fair and consistent comparison, our proposed local aggregation function is tested within the same architecture and framework as [24, 15]. The architecture in study is a U-Net inspired architecture consisting of encoder and decoder blocks. An illustration of the architecture is depicted in Figure 4.

Encoder Block: The architecture consists of five encoding blocks comprised of residual and strided residual blocks, each with 1×1 convolution operators and a local aggregation function within. The encoder block operates on hierarchical point cloud resolutions to incorporate contextual information at multiple scales. Going from one encoder layer to the other, point cloud resolution is reduced using point cloud subsampling methods. In order to account for the varying density problem commonly encountered in point clouds, [24] proposes to use grid-subsampling to reduce the resolution while maintaining a uniform point cloud density

throughout. The grid size is doubled going from an encoder layer to the subsequent one. The strided residual block acts as a graph pooling operation. It operates on the reduced point cloud as center points with neighbors queried in the preceding encoder point cloud at higher resolution. Neighbors are queried using ball neighborhood that retrieves a more representative neighbors as compared to the density sensitive k-nearest-neighbors [4]. The ball neighborhood radius is doubled going deeper in the encoder to account for the increasing sparsity of the point cloud due to downsampling. The features of lowest resolution at the end of the encoder block are propagated to the full cloud resolution by the decoder block.

Decoder Block: It consists of nearest neighbor interpolation and 1×1 convolution operations. Nearest neighbor interpolation copies the features of points at low resolution to their neighbors in the subsequent decoder point cloud at higher resolution. Skip connections inject encoder features at the same resolution as upsampled decoder features. The two are concatenated and merged by a 1×1 convolution operator. [15] introduces the parameter C as the output channel dimension of the first local aggregation function as a way to control the size of the model.

4. Experiments

To demonstrate the effectiveness of our proposed local aggregation function, we evaluate models under the same settings proposed in [24, 15] for the task of indoor scene semantic segmentation and [15] for shape part segmentation.

4.1. Indoor Scene Semantic Segmentation

We conduct experiments on two large-scale, indoor scene semantic segmentation datasets: S3DIS [1] and ScanNet [2]. The output feature dimension of first local aggregation is set to $C = 36$ as proposed for the small model variants in [15]. On S3DIS, ZRGB1 point features are used as initial inputs to the model following [24, 15]. On Scan-

Method	S3DIS A5	S3DIS 6F	ScanNet
PointNet [18]	41.1	-	-
PointNet++ [20]	-	-	33.9
PointCNN [13]	57.5	65.4	45.8
SSP+SPG [7]	61.7	68.4	-
SPH3D-GCN [10]	59.5	68.9	61.0
SegGCN [9]	63.6	68.5	58.9
PointASNL [30]	62.6	68.7	66.6
RandLANet [5]	-	70.0	-
PointwiseMLP (25.5M) [15]	66.2	-	-
Pseudo Grid (18.5M) [15]	65.9	-	-
PosPool* (18.5M)[15]	66.7	-	-
KPConv (r) (14.1M)[24]	65.4	69.6	68.6
KPConv (d) (14.9M)[24]	67.1	70.6	68.4
2 groups - SALANet (1.6M)	67.6	72.5	67.0

Table 1. **State-of-the-art mIoU comparison on S3DIS and ScanNet.** SALANet with $S = 2$ groups achieves SOTA on S3DIS test Area 5 (A5) and 6-fold-cross-validation (6F), and competitive performance on ScanNet test set in comparison with much bigger models. Only point processing methods are considered for ScanNet. **M** corresponds to million parameters.

Net, RGB1 features are used as in [24]. The concatenated “1” feature is meant to account for all black RGB points. The downsampling base grid size is set to 0.04 meters for both datasets. S3DIS [1] consists of six large areas of indoor scenes scanned using a Matterport device. Every point is defined with its XYZ coordinates, RGB color features, and a class label that takes one of thirteen different semantic classes. We report mean intersection over union (mIoU) on both Area 5 and 6-fold-cross-validation benchmarks to demonstrate the generalization of our proposed aggregation function. ScanNet [2] on the other hand consists of 1513 training scenes scanned using RGB-D cameras. Every point is defined with its XYZ coordinate, RGB color features, and a class label that takes one of twenty different semantic labels. The train/val split is set as suggested by the benchmark. The test set is comprised of 100 scenes. The reported mIoU metric is on the test set as reported on the ScanNet benchmarks hosting website.

In training on both datasets, random spheres are sampled with a radius $r = 2$ meters. In testing, overlapping spheres are sampled regularly, so that every point is inferred multiple times in different contexts as a voting scheme following [24, 15]. The multiple predictions are then averaged and a point label is assigned. SALANet refers to the model configured with SALA as local aggregation function. Results of SALANet on 3D scene semantic segmentation are summarized in Table 1. On S3DIS Area 5, SALANet with only $S = 2$ groups reaches 67.6 mIoU defining the new SOTA on this benchmark. Similarly, it reaches 72.5 mIoU on the 6-fold-cross-validation benchmark outperforming the current SOTA method by close to 2 mIoU points, while us-

Method	PartNet (mpIoU)
ResGCN28 [11]	45.1
PointCNN (4.4M)[13]	46.5
PointwiseMLP (C=36, 1.6M) [15]	47
Pseudo Grid (C=36, 1.2M) [15]	45.2
PosPool* (C=36, 1.1M) [15]	47.2
PointwiseMLP (C=144, 25.6M) [15]	51.2
Pseudo Grid (C=144, 18.5M) [15]	53
PosPool* (C=144, 18.5M) [15]	53.8
1 group - SALANet (C=36, 1.4M)	48.5
2 groups - SALANet (C=36, 1.6M)	49.4
2 groups - SALANet (C=72, 6.4M)	52.4

Table 2. **Shape Part Segmentation mpIoU on PartNet.** SALANet with $S = 2$ groups and $C = 72$ achieves competitive performance on PartNet (level 3) test set in comparison with much bigger models. SALANet is trained and tested under the same settings in [15]. **M** corresponds to million parameters.

ing $10\times$ less parameters. The bigger boost on the 6-fold-cross-validation demonstrates the generalization capability of our proposed local aggregation function. On ScanNet, SALANet reaches 67 mIoU with $9\times$ less parameters compared to the much more complex rigid kernel of KPConv [24]. This demonstrates the accuracy-to-efficiency balance of our proposed SALA function when compared to other SOTA methods. Sample qualitative results on S3DIS Area 5 are showcased in Figure 5.

4.2. 3D Shape Part Segmentation

We conduct further experiments on PartNet for the task of shape part segmentation. PartNet [17] is a large-scale dataset for part segmentation consisting of synthetic 3D CAD models with 24 shape categories, each with a different set of assembled parts. We consider the most fine-grained segmentation (level-3) task on this dataset, which involves 17 shape categories. We follow [15] by training on all categories at once instead of training different shapes independently. This is done by using the same backbone and an independent classifier head per shape category. We use XYZ1 features as model inputs and a base grid size of 0.02 meters. We follow the official train/val split and report mean part IoU (mpIoU) on the test set that comprises 20% of the entire dataset. Results of SALANet on 3D shape part segmentation are summarized in Table 2. On PartNet, we test SALANet with $C = 36$ and $S = 2$ groups and report 49.4 mpIoU on the test set. This small model variant outperforms all small model variants proposed in [15] (*i.e.* PointwiseMLP, Pseudo Grid, and PosPool with $C = 36$). To demonstrate the effectiveness of our aggregation function, we double the output channel size to $C = 72$ and show that our SALANet with $S = 2$ groups can reach a very competitive performance with almost $3\times$ times less parameters than the large model variants in [15] with $C = 144$.

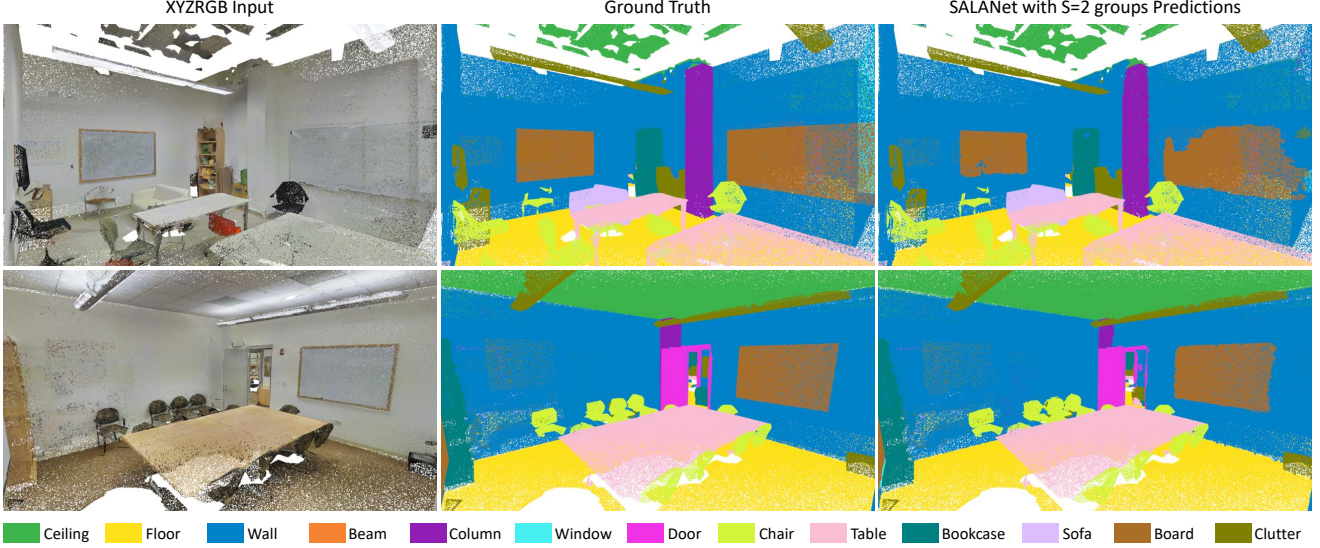


Figure 5. **Qualitative Results.** Sample qualitative results of SALANet with $S = 2$ groups on S3DIS Area 5. SALANet attends to easily confused classes such as wall/column, wall/board and wall/door that are all semantically similar.

The comparison is especially valuable with the Pseudo Grid method, which uses point kernel aggregation [24] with a geometric neighbor-to-grid assignment function. Moreover, SALANet with $S = 1$ group offers a better setting for a pointwise-MLP local aggregation as compared to the one proposed in [15]. This is reflected by a 1.5 mIoU boost over the PointwiseMLP model with fewer parameters. We note that increasing the value of C comes with a trade-off of potential overfitting, as well as a high price in terms of efficiency. We further explore these trade-offs in the supplementary material.

5. Ablations and Analysis

The adopted setting of SALANet uses $S = 2$ groups and $f_j^* = [r_j, f_j]$ (7) as input for local aggregation. We conduct an ablation study on the number of groups and possible variants of inputs to SALA (f_j^*). We test the resulting SALANet models on S3DIS Area 5. The results of the different SALANet configurations are summarized in Table 3.

Group Kernel Size. When reducing the number of groups to $S = 1$, the performance drops by 2 mIoU points to reach 65.5 mIoU. In doing so, SALA reduces to a pointwise-MLP local aggregation function. Nevertheless, SALANet with $S = 1$ outperforms many other SOTA methods on Area 5 with much less parameters. This includes the rigid kernel point method of KPconv [24] that uses $S = 15$ kernel weights. Similarly, a drop in performance is also observed when increasing the number of groups of SALANet to $S = 3$ and more (Table 4). We try and explain the discrepancy in performance between a complex kernel and a simple pointwise-MLP one by introducing the varying local neighbor diversity problem.

Method	SALA Input	S3DIS A5
PointNet++ [20]	$[p_{ij}, f_j]$	-
PointwiseMLP (C=36, 1.6M) [15]	$[p_{ij}, f_i, f_{ij}]$	56.7
PointwiseMLP (C=144, 25.5M) [15]	$[p_{ij}, f_i, f_{ij}]$	66.2
1 group - SALANet (C=36, 1.4M)	$[r_j, f_j]$	65.5
2 groups - SALANet ⁺ (C=36, 1.6M)	$[r_j, f_j]$	67.6
3 groups - SALANet (C=36, 1.8M)	$[r_j, f_j]$	65.7
1 group - SALANet (C=36, 1.4M)	$[p_{ij}, f_j]$	61.1
1 group - SALANet (C=36, 1.5M)	$[p_{ij}, f_i, f_{ij}]$	65.1
2 groups - SALANet (C=36, 1.6M)	$[p_{ij}, f_j]$	65.5
2 groups - SALANet (C=36, 1.8M)	$[p_{ij}, f_i, f_{ij}]$	66.4

Table 3. **Ablation of SALANet on S3DIS Area 5.** We report results of SALANet model variants using SALA with different numbers of groups and different aggregation inputs (f_j^*) on S3DIS test Area 5 (A5). The upper table sub-part corresponds to varying the number of groups and the lower sub-part corresponds to varying the choice of inputs. (+) denotes the configuration of choice. M corresponds to million parameters.

A semantically diverse neighborhood consists of neighbors with very different features. Grid-based methods take advantage of this diversity to model class interactions in order to improve feature learning. We conjecture that when there is too little local semantic diversity, grid-based methods are at a disadvantage. Having a larger grid kernel size may be overwhelming for some localities with low neighbor diversity. This is especially problematic early on in the encoder block, where the point cloud resolution is still relatively high. On the other hand, a complex kernel is necessary at class boundaries where a neighborhood is semantically diverse. This sheds the light on why increasing the number of groups in SALANet (beyond $S = 2$) results in

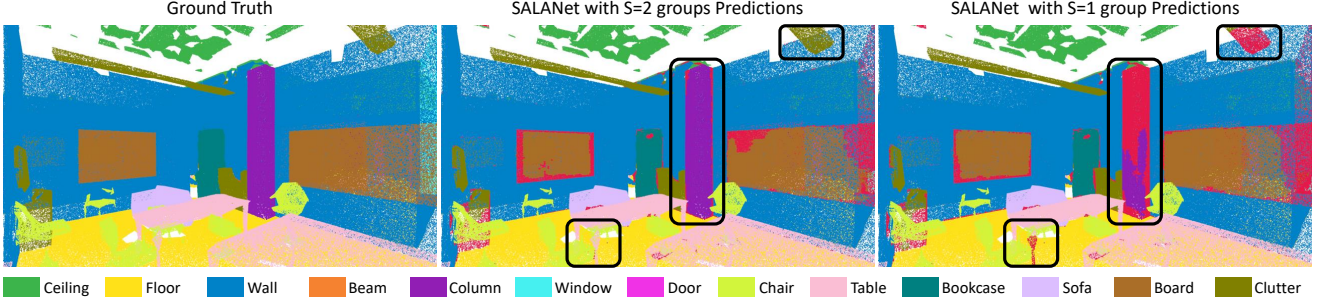


Figure 6. **Qualitative results comparison.** SALANet with $S = 2$ does particularly well on handling localities, where multiple classes interact. Examples of such encounters are column/wall and chair/table. SALANet with $S = 1$ better handles local label consistency at localities with low neighbor diversity, *e.g.* in the middle of a board instance. Misclassified points are highlighted in red for reference.

Method	mIoU	ceiling	floor	wall	beam	column	window	door	table	chair	sofa	book.	board	clutter
KPConv (r) (14.1M)[24]	65.4	92.6	97.3	81.4	0	16.5	54.5	69.5	80.2	90.1	66.4	74.6	63.7	58.1
KPConv (d) (14.9M)[24]	67.1	92.8	97.3	82.4	0	23.9	58	69	81.5	91	75.4	75.3	66.7	58.9
1 group - SALANet (1.4M)	65.5	95.5	98.3	81.5	0	9.2	56.3	63.1	82.1	89.9	75.5	75.5	62.2	62
2 groups - SALANet ⁺ (1.6M)	67.6	94.9	98.3	82.5	0	26.2	55	71.1	82.7	91.3	73.3	77.8	63.8	61.9
3 groups - SALANet (1.8M)	65.7	94.8	98.3	82.5	0	11.5	58.1	66.9	82.2	90.5	67.1	76.4	63.0	62.5

Table 4. **Comparison with KPConv on S3DIS Area 5.** We compare the per class IoU of KPConv [24] against that of SALANet with different group kernel settings. (+) denotes the configuration of choice. **M** corresponds to million parameters.

worse performance. Having too many groups can confuse the learnable assignment. This happens when the regressed assignment probabilities are comparable in magnitude. On the other hand, when there is not enough groups to capture all semantic interactions, it leads to a reduced performance on the task of semantic segmentation. This is reflected by the boost in the column and door class IoUs going from SALANet with $S = 1$ to $S = 2$ groups, followed by a drop with $S = 3$ groups as seen in Table 4. Qualitative results comparing the performance of SALANet with $S = 1$ to $S = 2$ are shown in Figure 6.

SALA Input. We experiment with two other inputs for our aggregation function to showcase the potency of using lifted relative positions for both better performance and efficiency.

We first replace the lifted relative position r_j with just relative position p_{ij} resulting in $f_j^* = [p_{ij}, f_j]$ input [20]. This results in a 2 mIoU point drop for SALANet with $S = 2$ groups and 4 mIoU point drop for the model with $S = 1$ group. We believe the benefit of using lifted relative position r_j is to decouple the neighbor search space from point feature learning. Moreover, using the lifted relative position will allow gradients a better flow back to the learnable assignment function to further improve the soft assignment process.

The effectiveness of a pointwise-MLP model in comparison with complex kernels have been demonstrated before in [15], but we further enforce it by arriving at a better setting for efficiency. PointwiseMLP model uses the center

point feature and relative neighbor feature instead of the absolute one $f_j^* = [p_{ij}, f_i, f_{ij}]$. Under the same local aggregation input f_j^* and output channel size $C = 36$, SALANet with $s = 1$ outperforms PointwiseMLP model with 8 mIoU points reaching 65.1 mIoU. Under both group kernel sizes $s = 1, 2$, our initial choice of inputs for SALA $f_j^* = [r_j, f_j]$ provides the best performance on semantic segmentation.

6. Conclusion

In this work, we presented SALA as an example of a grid-based local aggregation function that leverages a learnable neighbor-to-grid assignment. Instead of relying on a spatial grid, our local aggregation function softly assigns neighbor points to a fixed number of irregular, unstructured, and non-spatial groups. We integrate our local aggregation in a deeper architecture, SALANet, designed for 3D semantic segmentation. We demonstrate the impact of a learnable mapping by achieving SOTA results on S3DIS and competitive performance on ScanNet and PartNet, while using a fraction of the parameters used in SOTA methods. The learned assignment has the flexibility to adapt per layer and locality, and it is driven by the performance on the end task of semantic segmentation. The number of groups is chosen to be fixed per layer, but future work could extend to adaptive group sizes.

References

- [1] Iro Armeni, Sasha Sax, Amir R Zamir, and Silvio Savarese. Joint 2d-3d-semantic data for indoor scene understanding. *arXiv preprint arXiv:1702.01105*, 2017. 5, 6
- [2] Angela Dai, Angel X Chang, Manolis Savva, Maciej Halber, Thomas Funkhouser, and Matthias Nießner. Scannet: Richly-annotated 3d reconstructions of indoor scenes. In *Proceedings of the IEEE Conference on Computer Vision and Pattern Recognition*, pages 5828–5839, 2017. 5, 6
- [3] Benjamin Graham, Martin Engelcke, and Laurens Van Der Maaten. 3d semantic segmentation with submanifold sparse convolutional networks. In *Proceedings of the IEEE conference on computer vision and pattern recognition*, pages 9224–9232, 2018. 2
- [4] Pedro Hermosilla, Tobias Ritschel, Pere-Pau Vázquez, Àlvar Vinacua, and Timo Ropinski. Monte carlo convolution for learning on non-uniformly sampled point clouds. *ACM Transactions on Graphics (TOG)*, 37(6):1–12, 2018. 5
- [5] Qingyong Hu, Bo Yang, Linhai Xie, Stefano Rosa, Yulan Guo, Zhihua Wang, Niki Trigoni, and Andrew Markham. Randla-net: Efficient semantic segmentation of large-scale point clouds. *Proceedings of the IEEE Conference on Computer Vision and Pattern Recognition*, 2020. 3, 6, 13
- [6] Abhijit Kundu, Xiaoqi Yin, Alireza Fathi, David Ross, Brian Brewington, Thomas Funkhouser, and Caroline Pantofaru. Virtual multi-view fusion for 3d semantic segmentation. *arXiv preprint arXiv:2007.13138*, 2020. 2
- [7] Loïc Landrieu and Mohamed Boussaha. Point cloud over-segmentation with graph-structured deep metric learning. In *Proceedings of the IEEE Conference on Computer Vision and Pattern Recognition*, pages 7440–7449, 2019. 6, 12, 13
- [8] Felix Järemo Lawin, Martin Danelljan, Patrik Tostenberg, Goutam Bhat, Fahad Shahbaz Khan, and Michael Felsberg. Deep projective 3d semantic segmentation. In *International Conference on Computer Analysis of Images and Patterns*, pages 95–107. Springer, 2017. 2
- [9] Huan Lei, Naveed Akhtar, and Ajmal Mian. Seggen: Efficient 3d point cloud segmentation with fuzzy spherical kernel. In *Proceedings of the IEEE Conference on Computer Vision and Pattern Recognition*, pages 11611–11620, 2020. 2, 3, 6, 12, 13
- [10] Huan Lei, Naveed Akhtar, and Ajmal Mian. Spherical kernel for efficient graph convolution on 3d point clouds. *IEEE Transactions on Pattern Analysis and Machine Intelligence*, 2020. 2, 3, 6, 12, 13
- [11] Guohao Li, Matthias Müller, Guocheng Qian, Itzel C Delgadillo, Abdullellah Abualshour, Ali Thabet, and Bernard Ghanem. Deepgcns: Making gcns go as deep as cnns. *arXiv preprint arXiv:1910.06849*, 2019. 6, 13
- [12] Guohao Li, Matthias Muller, Ali Thabet, and Bernard Ghanem. Deepgcns: Can gcns go as deep as cnns? In *Proceedings of the IEEE International Conference on Computer Vision*, pages 9267–9276, 2019. 3, 12
- [13] Yangyan Li, Rui Bu, Mingchao Sun, Wei Wu, Xinhan Di, and Baoquan Chen. Pointcnn: Convolution on x-transformed points. In *Advances in neural information processing systems*, pages 820–830, 2018. 6, 12, 13
- [14] Yongcheng Liu, Bin Fan, Shiming Xiang, and Chunhong Pan. Relation-shape convolutional neural network for point cloud analysis. In *Proceedings of the IEEE Conference on Computer Vision and Pattern Recognition*, pages 8895–8904, 2019. 3
- [15] Ze Liu, Han Hu, Yue Cao, Zheng Zhang, and Xin Tong. A closer look at local aggregation operators in point cloud analysis. *ECCV*, 2020. 2, 5, 6, 7, 8, 11, 12, 13
- [16] Daniel Maturana and Sebastian Scherer. Voxnet: A 3d convolutional neural network for real-time object recognition. In *2015 IEEE/RSJ International Conference on Intelligent Robots and Systems (IROS)*, pages 922–928. IEEE, 2015. 1, 2
- [17] Kaichun Mo, Shilin Zhu, Angel X Chang, Li Yi, Subarna Tripathi, Leonidas J Guibas, and Hao Su. Partnet: A large-scale benchmark for fine-grained and hierarchical part-level 3d object understanding. In *Proceedings of the IEEE Conference on Computer Vision and Pattern Recognition*, pages 909–918, 2019. 6
- [18] Charles R Qi, Hao Su, Kaichun Mo, and Leonidas J Guibas. Pointnet: Deep learning on point sets for 3d classification and segmentation. In *Proceedings of the IEEE conference on computer vision and pattern recognition*, pages 652–660, 2017. 3, 6, 12, 13
- [19] Charles R Qi, Hao Su, Matthias Nießner, Angela Dai, Mengyuan Yan, and Leonidas J Guibas. Volumetric and multi-view cnns for object classification on 3d data. In *Proceedings of the IEEE conference on computer vision and pattern recognition*, pages 5648–5656, 2016. 2
- [20] Charles Ruizhongtai Qi, Li Yi, Hao Su, and Leonidas J Guibas. Pointnet++: Deep hierarchical feature learning on point sets in a metric space. In *Advances in neural information processing systems*, pages 5099–5108, 2017. 3, 6, 7, 8, 13
- [21] Gernot Riegler, Ali Osman Ulusoy, and Andreas Geiger. Octnet: Learning deep 3d representations at high resolutions. In *Proceedings of the IEEE Conference on Computer Vision and Pattern Recognition*, pages 3577–3586, 2017. 2
- [22] Hang Su, Subhransu Maji, Evangelos Kalogerakis, and Erik Learned-Miller. Multi-view convolutional neural networks for 3d shape recognition. In *Proceedings of the IEEE international conference on computer vision*, pages 945–953, 2015. 1, 2
- [23] Maxim Tatarchenko, Jaesik Park, Vladlen Koltun, and Qian-Yi Zhou. Tangent convolutions for dense prediction in 3d. In *Proceedings of the IEEE Conference on Computer Vision and Pattern Recognition*, pages 3887–3896, 2018. 2
- [24] Hugues Thomas, Charles R Qi, Jean-Emmanuel Deschaud, Beatriz Marcotequi, François Goulette, and Leonidas J Guibas. Kpconv: Flexible and deformable convolution for point clouds. In *Proceedings of the IEEE International Conference on Computer Vision*, pages 6411–6420, 2019. 2, 3, 4, 5, 6, 7, 8, 11, 12, 13
- [25] Petar Veličković, Guillem Cucurull, Arantxa Casanova, Adriana Romero, Pietro Lio, and Yoshua Bengio. Graph attention networks. *arXiv preprint arXiv:1710.10903*, 2017. 3

- [26] Lei Wang, Yuchun Huang, Yaolin Hou, Shenman Zhang, and Jie Shan. Graph attention convolution for point cloud semantic segmentation. In *Proceedings of the IEEE Conference on Computer Vision and Pattern Recognition*, pages 10296–10305, 2019. 3, 12
- [27] Peng-Shuai Wang, Yang Liu, Yu-Xiao Guo, Chun-Yu Sun, and Xin Tong. O-cnn: Octree-based convolutional neural networks for 3d shape analysis. *ACM Transactions on Graphics (TOG)*, 36(4):1–11, 2017. 2
- [28] Yue Wang, Yongbin Sun, Ziwei Liu, Sanjay E Sarma, Michael M Bronstein, and Justin M Solomon. Dynamic graph cnn for learning on point clouds. *Acm Transactions On Graphics (tog)*, 38(5):1–12, 2019. 3
- [29] Wenxuan Wu, Zhongang Qi, and Li Fuxin. Pointconv: Deep convolutional networks on 3d point clouds. In *Proceedings of the IEEE Conference on Computer Vision and Pattern Recognition*, pages 9621–9630, 2019. 3
- [30] Xu Yan, Chaoda Zheng, Zhen Li, Sheng Wang, and Shuguang Cui. Pointasnl: Robust point clouds processing using nonlocal neural networks with adaptive sampling. In *Proceedings of the IEEE/CVF Conference on Computer Vision and Pattern Recognition*, pages 5589–5598, 2020. 6, 12, 13
- [31] Feihu Zhang, Jin Fang, Benjamin Wah, and Philip Torr. Deep fusionnet for point cloud semantic segmentation. *ECCV*, 2020. 2

Supplementary Material

A. Architecture Blocks

Residual and Strided Residual architecture blocks are detailed in Figure 7 as in [15].

B. Training and Inference Settings

We evaluate Soft Assignment Local Aggregation (SALA) function in the unified framework proposed in [15]. This includes data pre-processing, augmentation, architecture (see Figure 7), and training and inference schemes. Models are trained with cross-entropy loss and L_2 regularizer on learned weights.

B.1. S3DIS

The initial inputs to the model are lifted ZRGB1 features ($d_0 = 5$). Following [15, 24], the data is augmented with random rotations along the z-axis, random scaling (ratios 0.7 to 1.3), random color drop, and additive Gaussian point perturbations with standard deviation $\delta = 0.001$. The reported mIoU is a result of voting scheme employed in [15, 24]. A point cloud is divided using regular overlapping spheres. The logits of a point seen in different spheres are then averaged before Softmax and label assignment.

B.2. ScanNet

The initial inputs to the model are lifted RGB1 features ($d_0 = 4$). Following [24], the data is augmented with random rotations along the z-axis, random scaling (ratios 0.9 to 1.1), random color drop, and additive Gaussian point perturbations with standard deviation $\delta = 0.001$. The reported mIoU is as reported on ScanNet benchmarks website. Predictions on the test-set are collected using the same voting scheme discussed previously as in [24].

B.3. PartNet

The initial inputs to the model are lifted XYZ1 features ($d_0 = 4$). Following [15], the data is augmented with random scaling (ratios 0.8 to 1.2), and additive Gaussian point perturbations with standard deviation $\delta = 0.001$. The reported mIoU is a result of voting scheme where logits are averaged over prediction on augmented test-set as in [15].

C. Quantitative and Qualitative Results

C.1. S3DIS

Tables 5 and 6 show the per class IoU on S3DIS Area 5 and 6-fold-cross-validation benchmarks respectively. On both benchmarks, SALANet with $S = 2$ groups achieves state-of-the-art (SOTA) performance. Sample qualitative results are showcased in Figure 8.

C.2. ScanNet

Table 7 shows the per class IoU on ScanNet test-set. SALANet with $S = 2$ groups achieves competitive performance while using much less parameters in comparison with other SOTA methods with much more complex kernels. Sample qualitative results on validation-set are showcased in Figure 9.

C.3. PartNet

Table 8 shows the per shape category mean part IoU (mpIoU) on PartNet test-set. [15] noted that increasing the output channel dimension C is especially important on complex datasets such as PartNet. We vary the output channel dimension C to test our model at different model learning capacities. Increasing the channel dimension compromises the efficiency of SALANet and does not consistently yield an improvement on the general performance. This could be a result of potential overfitting. Yet, SALANet with $S = 2$ groups achieves competitive performance in comparison with much larger models. Sample qualitative results on test-set are showcased in Figure 10.

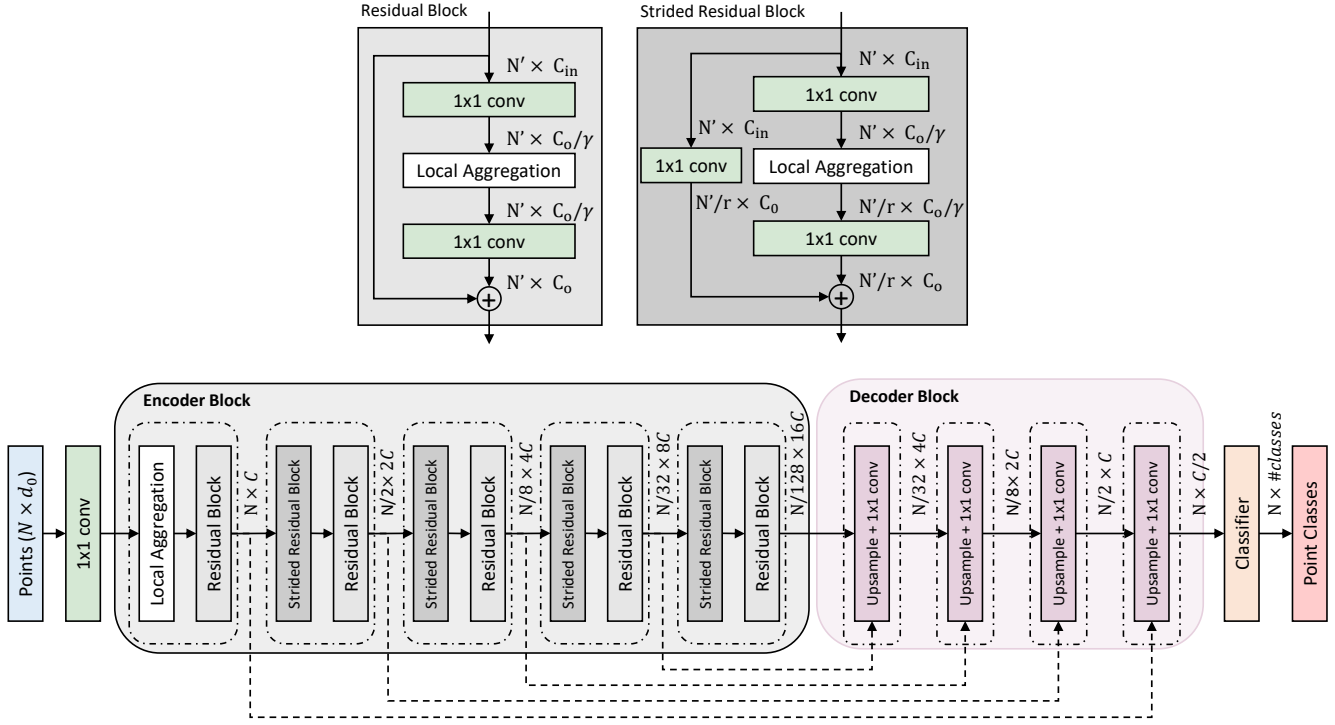


Figure 7. **Architecture.** Unified architecture framework from [15]. Both Residual and Strided Residual Blocks have local aggregation functions within. The strided residual blocks acts as a pooling operator in which point cloud resolution is reduced using grid-subsampling. The grid size is doubled going deeper in the encoder. C refers to channel output of first encoding layer. $\gamma = 2$ is the residual bottleneck ratio. r refers to the encoder point cloud downsampling ratio.

Semantic Segmentation on S3DIS Area 5														
Method	mIoU	ceiling	floor	wall	beam	column	window	door	table	chair	sofa	book.	board	clutter
PointNet [18]	41.1	88.8	97.3	69.8	0	3.9	46.3	10.8	52.6	58.9	40.3	5.9	26.4	33.2
ResGCN28 [12]	52.5	-	-	-	-	-	-	-	-	-	-	-	-	-
PointCNN [13]	57.3	92.3	98.2	79.4	0	17.6	22.8	62.1	74.4	80.6	31.7	66.7	62.1	56.7
SSP+SPG [7]	61.7	-	-	-	-	-	-	-	-	-	-	-	-	-
SPH3D-GCN [10]	59.5	93.3	97.1	81.1	0	33.2	45.8	43.8	79.7	86.9	33.2	71.5	54.1	53.7
SegGCN [9]	63.6	93.7	98.6	80.6	0	28.5	42.6	74.5	80.9	88.7	69.0	71.3	44.4	54.3
PointASNL [30]	62.6	94.3	98.4	79.1	0	26.7	55.2	66.2	83.3	86.8	47.6	68.3	56.4	52.1
GACNet [26]	62.9	92.3	98.3	81.9	0	20.4	59.1	40.9	78.5	85.8	61.7	70.8	74.7	52.8
PointwiseMLP(25.6M) [15]	66.2	93	98.4	82.1	0	18.5	59.1	63	83.5	91.1	76.4	76	62.5	57.3
Pseudo Grid (18.5M) [15]	65.9	94	98.4	82.6	0	20	55.7	65.2	81.5	91.5	65.3	76.3	66.7	60.1
PosPool* (18.5M) [15]	66.7	94.9	98.4	82.5	0	24	51.8	70.6	82.3	92	68.1	76.7	65	61.1
KPConv (r) (14.1M)[24]	65.4	92.6	97.3	81.4	0	16.5	54.5	69.5	80.2	90.1	66.4	74.6	63.7	58.1
KPConv (d) (14.9M)[24]	67.1	92.8	97.3	82.4	0	23.9	58	69	81.5	91	75.4	75.3	66.7	58.9
1 group - SALANet (1.4M)	65.5	95.5	98.3	81.5	0	9.2	56.3	63.1	82.1	89.9	75.5	75.5	62.2	62
2 groups - SALANet (1.6M)	67.6	94.9	98.3	82.5	0	26.2	55	71.1	82.7	91.3	73.3	77.8	63.8	61.9
3 groups - SALANet (1.8M)	65.7	94.8	98.3	82.5	0	11.5	58.1	66.9	82.2	90.5	67.1	76.4	63.0	62.5

Table 5. **Scene semantic segmentation mIoU comparison on S3DIS Area 5.** SALANet with $S = 2$ groups achieves SOTA on S3DIS Area 5 while using close to $10\times$ less parameters than the reigning method. SALANet is trained and tested under the same settings in [15, 24]. **M** corresponds to million parameters.

Semantic Segmentation on S3DIS 6-Fold-Cross-Validation																
Method	OA	mAcc	mIoU	ceiling	floor	wall	beam	column	window	door	table	chair	sofa	book.	board	clutter
PointCNN [13]	88.1	75.6	65.4	94.8	97.3	75.8	63.3	51.7	58.4	57.2	71.6	69.1	39.1	61.2	52.2	58.6
SSP+SPG [7]	87.9	78.3	68.4	-	-	-	-	-	-	-	-	-	-	-	-	-
SPH3D-GCN [10]	88.6	77.9	68.9	93.3	96.2	81.9	58.6	55.9	55.9	71.7	72.1	82.4	48.5	64.5	54.8	60.4
SegGCN [9]	87.8	77.1	68.5	92.5	97.6	78.9	44.6	58.2	53.7	67.3	74.6	83.9	68	65.7	46.8	58.5
PointASNL [30]	88.8	79	68.7	95.3	97.9	81.9	47	48	67.3	70.5	71.3	77.8	50.7	60.4	63	62.8
RandLA-Net [5]	88	82	70	93.1	96.1	80.6	62.4	48	64.4	69.4	69.4	76.4	60	64.2	65.9	60.1
KPConv (r)(14.1M) [24]	-	78.1	69.6	93.7	92	82.5	62.5	49.5	65.7	77.3	64	57.8	71.7	68.8	60.1	59.6
KPConv (d)(14.9M) [24]	-	79.1	70.6	93.6	92.4	83.1	63.9	54.3	66.1	76.6	57.8	64	69.3	74.9	61.3	60.1
2 groups - SALANet (1.6M)	89.9	80.6	72.5	94.6	96.6	82.6	66.9	51.7	66.3	79.2	75.6	75.7	62.9	71.3	54.9	64.5

Table 6. **Scene semantic segmentation mIoU comparison on S3DIS 6-fold-cross-validation.** SALANet with $S = 2$ groups achieves SOTA on S3DIS 6-fold-cross-validation benchmark, outperforming the reigning method with almost 2 mIoU points while using close to $10\times$ less parameters. SALANet is trained and tested under the same settings in [15, 24]. M corresponds to million parameters.

Semantic Segmentation on ScanNet																		
Methods	mIoU	floor	wall	chair	sofa	table	door	cab	bed	desk	toil	sink	wind	pic	bkslhf	curt	show	cntr
PointCNN [13]	45.8	94.4	70.9	71.5	54.5	45.6	31.9	32.1	61.1	32.8	75.5	48.4	47.5	16.4	35.6	37.6	22.9	29.9
SPH3D-GCN [10]	61	93.5	77.3	79.2	70.5	54.9	50.7	53.2	77.2	57	85.9	60.2	53.4	4.6	48.9	64.3	70.2	40.4
SegGCN[9]	58.9	93.6	77.1	78.9	70	56.3	48.4	51.4	73.1	57.3	87.4	59.4	49.3	6.1	53.9	46.7	50.7	44.8
PointASNL [30]	66.6	95.1	80.6	83.0	75.1	55.3	53.7	65.5	78.1	47.4	81.6	67.5	70.3	27.9	75.1	76.9	69.8	47.1
KPConv (14.9M) [24]	68.4	93.5	81.9	81.4	78.5	61.4	59.4	64.7	75.8	60.5	88.2	69	63.2	18.1	78.4	77.2	80.5	47.3
2 groups - SALANet (1.6M)	67.0	92.4	79.4	80.7	74.6	62.3	54.5	65.2	77.0	65.9	89.2	63.5	57.0	14.9	76.8	74.7	81.1	45.1

Table 7. **Scene semantic segmentation mIoU comparison on ScanNet.** SALANet with $S = 2$ groups achieves competitive performance with much bigger and complex kernels on ScanNet test set while using almost $10\times$ less parameters. SALANet is trained and tested under the same settings in [24]. M corresponds to million parameters.

Part Segmentation on PartNet																		
Methods	mpIoU	Bed	Bottle	Chair	Clock	Dishws	Display	Door	Earph	Faucet	Knife	Lamp	Microw	Refriger	StrgFur	Table	Trsh	Can
PointNet [18]	35.6	13.4	29.5	27.8	28.4	48.9	76.5	30.4	33.4	47.6	32.9	18.9	37.2	33.5	38	29	34.8	44.4
PointNet++ [20]	42.5	30.3	41.4	39.2	41.6	50.1	80.7	32.6	38.4	52.4	34.1	25.3	48.5	36.4	40.5	33.9	46.7	49.8
ResGCN28 [11]	45.1	35.9	49.3	41.1	33.8	56.2	81	31.1	45.8	52.8	44.5	23.1	51.8	34.9	47.2	33.6	50.8	54.2
PointCNN [13]	46.5	41.9	41.8	43.9	36.3	58.7	82.5	37.8	48.9	60.5	34.1	20.1	58.2	42.9	49.4	21.3	53.1	58.9
PointwiseMLP(C=36, 1.6M) [15]	47.0	-	-	-	-	-	-	-	-	-	-	-	-	-	-	-	-	-
Pseudo Grid (C=36, 1.2M) [15]	45.2	-	-	-	-	-	-	-	-	-	-	-	-	-	-	-	-	-
PosPool* (C=36, 1.1M) [15]	47.2	-	-	-	-	-	-	-	-	-	-	-	-	-	-	-	-	-
PointwiseMLP(C=144, 25.6M) [15]	51.2	44.5	52.6	46.0	38.4	68.2	82.5	46.9	47.1	58.7	43.8	26.4	59.2	48.7	52.5	41.3	55.4	57.3
Pseudo Grid (C=144, 18.5M) [15]	53	47.5	50.9	49.2	44.9	67	84.2	49.1	49.9	62.8	38.3	27	59.4	54.3	54.1	44.5	57.4	60.7
PosPool* (C=144, 18.5M)[15]	53.8	49.5	49.4	48.3	49	65.6	84.2	56.8	53.8	62.4	39.3	24.7	61.3	55.5	54.6	44.8	56.9	58.2
1 group - SALANet (C=36, 1.4M)	48.5	43.7	45.7	44.4	35	63.5	80.2	41.2	47.3	52.1	44	26.9	54.6	47.3	47.6	40.3	53.3	57.9
2 groups - SALANet (C=36, 1.6M)	49.4	46.5	44.7	45	44.7	65.0	81.7	39.9	49.5	50.6	44.2	26.3	54.6	49.0	47.8	39.5	51.4	59.4
3 groups - SALANet (C=36, 1.8M)	48.9	44.3	47.2	44.7	34.2	65.9	81.6	38.9	45.4	57.0	43.8	24.6	52.5	51.2	49.0	40.6	54.2	56.6
2 groups - SALANet (C=72, 6.4M)	52.4	46.7	51.6	46.2	42.5	66.8	84.0	46.9	53.1	57.8	46.0	26.4	57.3	52.9	52.3	42.7	56.3	61.3
2 groups - SALANet (C=90, 10M)	53.1	46.9	55.7	45.8	48.5	67.4	82.8	50.5	50.1	57.6	45.8	25.8	58.4	54.8	53.0	43.3	57.4	59.5
2 groups - SALANet (C=120, 17.8M)	52.3	44.6	51.0	46.8	41.1	63.3	83.7	52.8	50.4	60.1	49.9	24.1	57.1	52.7	51.0	42.0	57.2	61.2

Table 8. **Shape part segmentation mpIoU comparison on PartNet.** SALANet with $S = 2$ groups and $C = 72$ achieves competitive performance on PartNet (level 3) test set in comparison with much bigger models. SALANet is trained and tested under the same settings in [15]. M corresponds to million parameters.

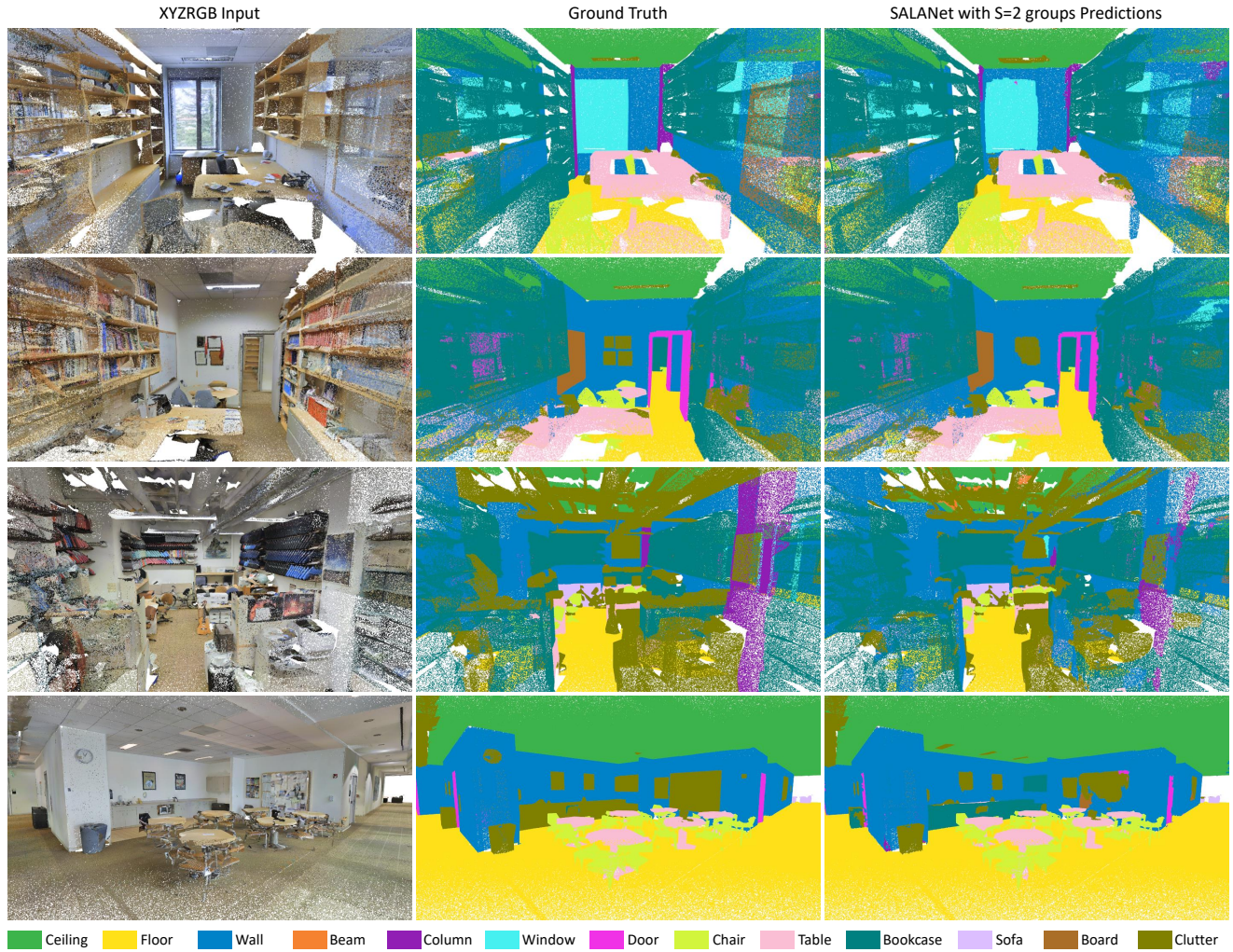


Figure 8. **Qualitative Results on S3DIS.** Sample qualitative results of SALANet with $S = 2$ groups on S3DIS Area 5.

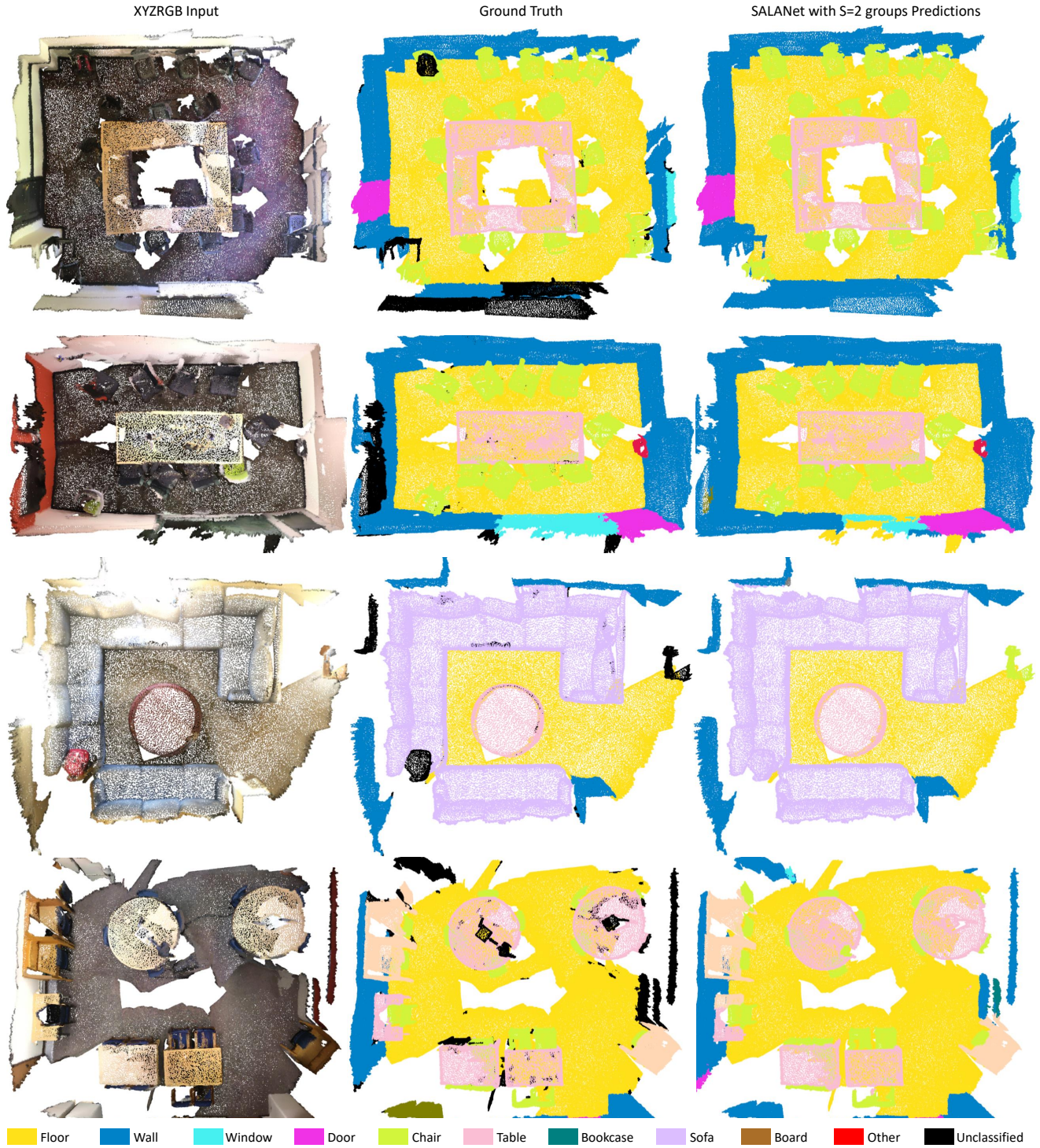


Figure 9. **Qualitative Results on ScanNet.** Sample qualitative results of SALANet with $S = 2$ groups on ScanNet validation-set.

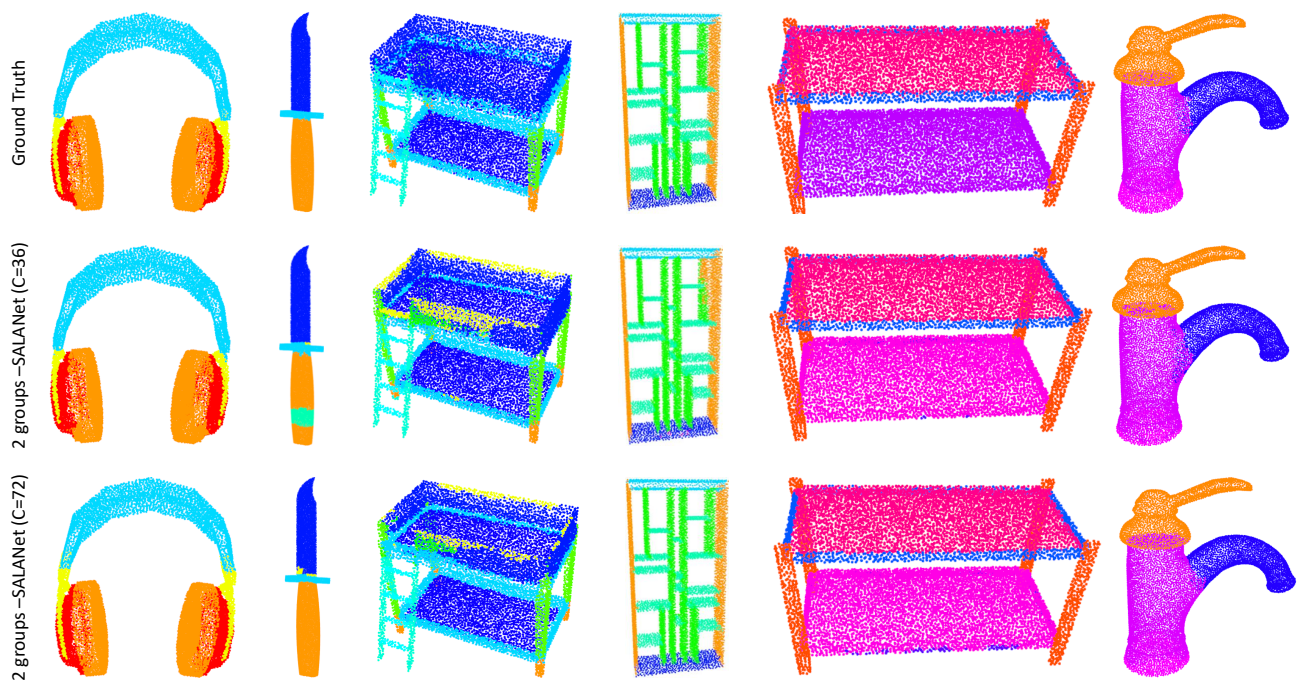


Figure 10. **Qualitative Results on PartNet.** Sample qualitative results of SALANet with $S = 2$ groups on PartNet test-set using output channel dimension $C = 36$ and $C = 72$